

Supporting Information

Ultra-broadband, Ultraviolet to Terahertz and High Sensitivity $\text{CH}_3\text{NH}_3\text{PbI}_3$ Perovskite Photodetectors

Yifan Li †, *Yating Zhang**†, *Tengteng Li* †, *Mengyao Li* †, *Zhiliang Chen* †, *Qingyan Li* †, *Hongliang Zhao* †, *Quan Sheng* †, *Wei Shi* †, and *Jianquan Yao**†

† Key Laboratory of Optoelectronics Information Technology, Ministry of Education, School of Precision Instruments and Optoelectronics Engineering, Tianjin University, Tianjin 300072, China

KEYWORDS: Ultra-broadband, photodetector, $\text{CH}_3\text{NH}_3\text{PbI}_3$ film, terahertz band, bolometric effect

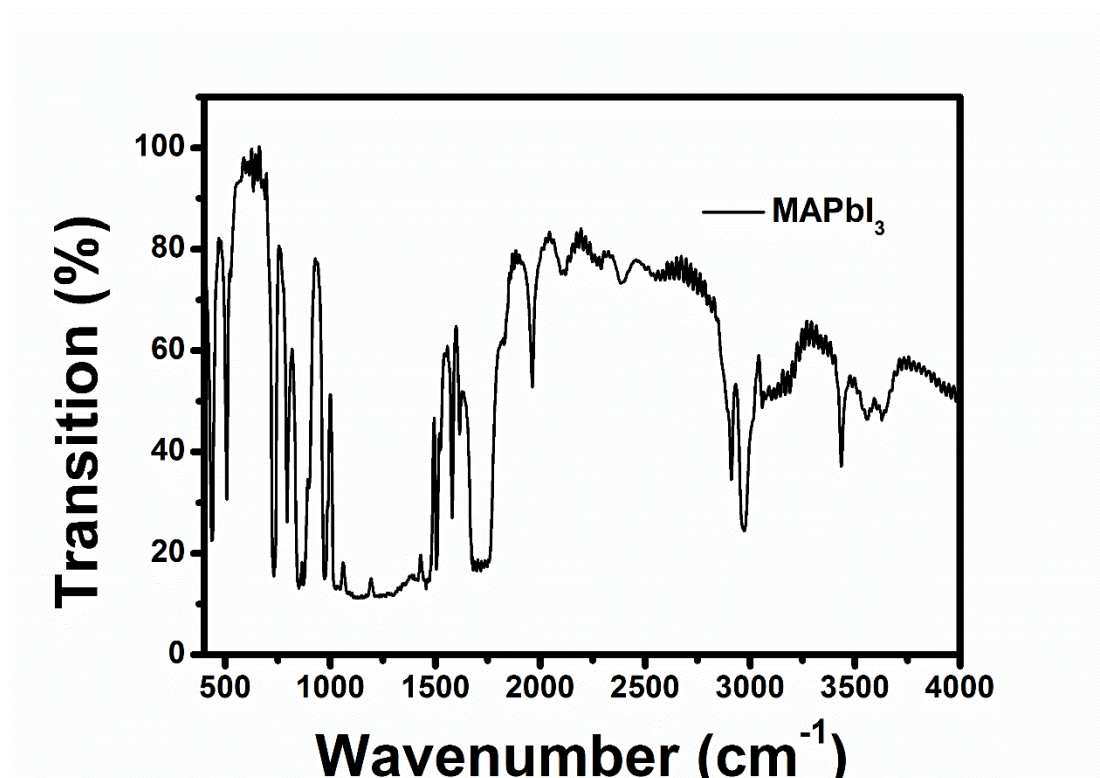


Figure S1 Infrared spectrum of MAPbI₃ film using Fourier Transform Infrared (FTIR).

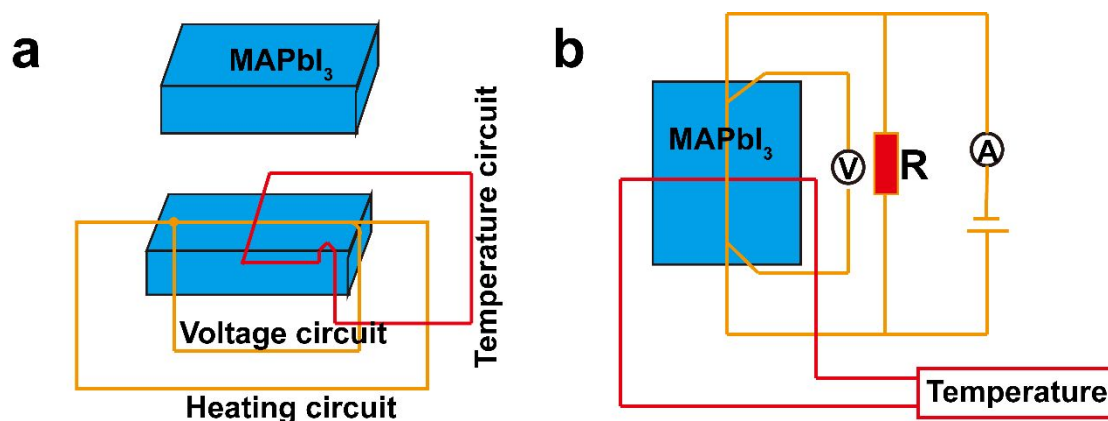


Figure S2 Schematic diagram of the thermal conductivity measurement structure (a) The mechanism of double-sample cross wire method. (b) Circuit connection diagram of double-sample cross wire method.

For thermoelectric photodetectors, thermal conductivity and Seebeck coefficients are significant parameters. The thermal conductivity value of $0.45 \text{ W m}^{-1}\text{K}^{-1}$ was measured by double-sample cross wire method¹, the schematic diagram of the measurement structure is shown in **Figure S2**. As shown in **Figure S2**, keep the sample

at the specified temperature, then a linear electrical conductor is buried between the surfaces of two samples. The thermal conductivity of the sample was calculated by measuring the temperature changes at two time points. Then the thermal conductivity can be calculated by the formula (1)

$$\kappa = \frac{VI}{4\pi} \times \frac{\ln(t_2/t_1)}{\Delta T_2 - \Delta T_1} \quad (1)$$

Where κ is the thermal conductivity, W/(mK); V is the voltage drop per unit length of the hot wire, V/m; I is the current, A; t_1 and t_2 are the test time, min; ΔT_1 and ΔT_2 are temperature rise of the hot wire, K.

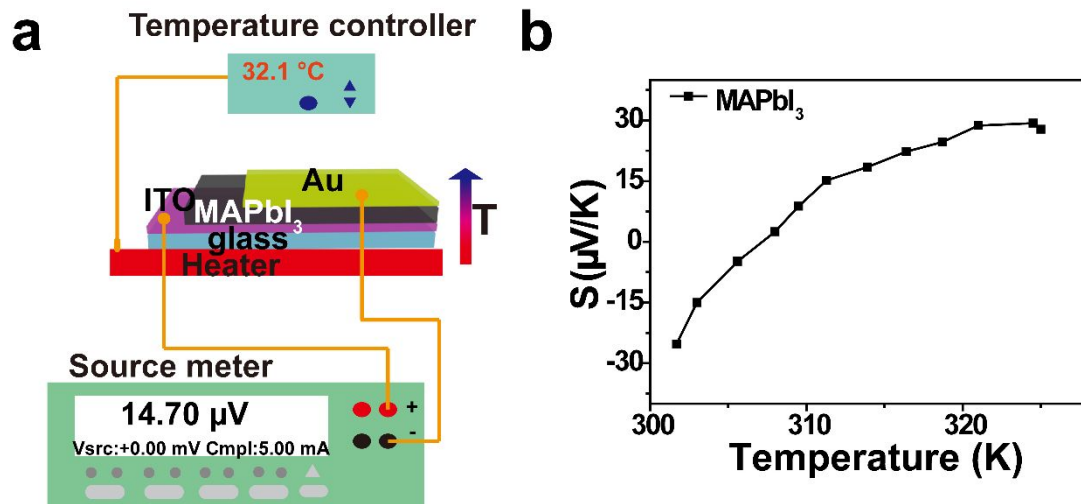


Figure S3 (a) Schematic of the Seebeck coefficient measurement experiment. (b) Seebeck coefficient of the MAPbI₃ perovskite under different heating temperature.

To acquired the Seebeck value of MAPbI₃ perovskite, the Seebeck coefficient measurement experiment was conduct. The structure of experimental equipment is shown in **Figure S3a**. The bottom of the device was heated by a heater band, The voltage difference (ΔV) between the two electrodes was measured by a Keithley 2400 source meter and the temperature distribution was obtained by the Infrared thermal imager (FLIR T630sc). The Seebeck coefficient was calculated as $S = \Delta V / \Delta T$, here S is the Seebeck coefficient, $\Delta T = T_{hot} - T_{cold}$, meaning the temperature difference

between hot side and cold side. **Figure S3b** shows the Seebeck coefficient of MAPbI₃ under different heating temperature. The Seebeck coefficient improves with the increase of temperature and then decreases, and exhibits the inflection point at 52 °C with the maximum Seebeck value of 29 μV K⁻¹. The results is consistent with the reported values by Ling Xu².

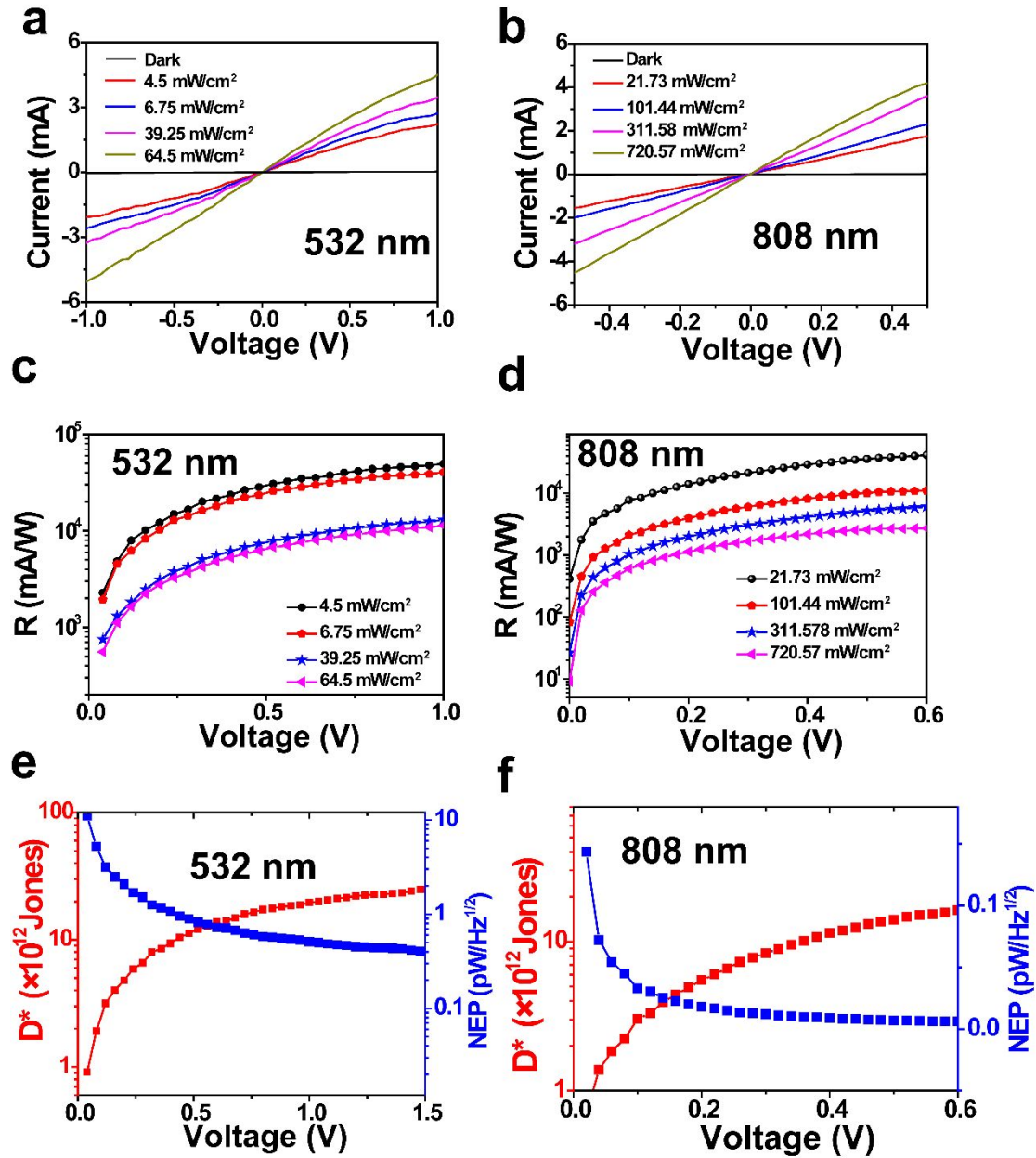


Figure S4 Photoelectric response characteristics of the MAPbI₃ photodetector under different illumination irradianations at 532 nm and 808 nm

Figure S4 shows the photoelectric response characteristics of the MAPbI₃ photodetector under different illumination irradianations at 532 nm and 808 nm. The photocurrents increase with the enhanced power intensity indicating that the photoexcited carriers increased with the increasing laser intensity. The photocurrent is well known to be attributed to the electron-hole pair generation excited by incident light with higher energy than the band gap of material. Incident light with sufficiently high

energy can excite more electrons from the valence band to the conduction band and cause a remarkable increase in carriers, which then contributes to photocurrent.

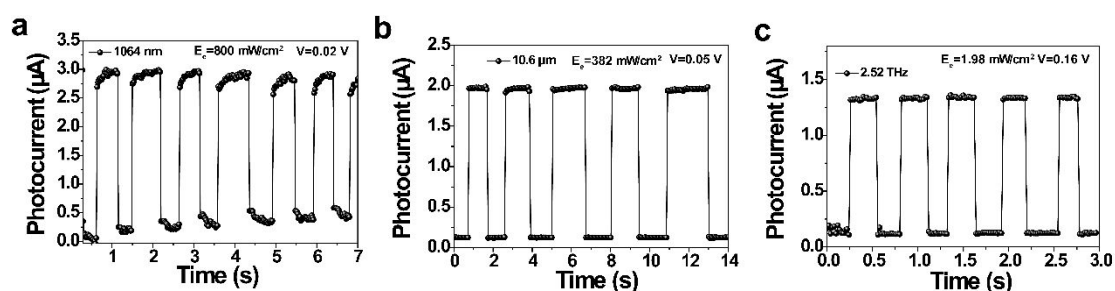


Figure S5 Multiple optical switch cycles of the device under 1064 nm, 10.6 μm and 118 μm (2.52 THz) illumination.

Figure S5 shows the Multiple optical switch cycles of the device under 1064 nm, 10.6 μm and 118 μm (2.52 THz) illumination. This can be explained, in the wavelength range from 400 to 810 nm, owing to the incident light energy is greater than that of the MAPbI₃ band gap, the absorption of photon energy mainly depends on the electron interband transition, so the PD shows a high absorption. However, at wavelengths beyond 810 nm, the laser energy is lower than that of the optical band gap, and the absorption of the photon energy is it mainly reliant on hot electrons, so the PD expresses a low absorption.

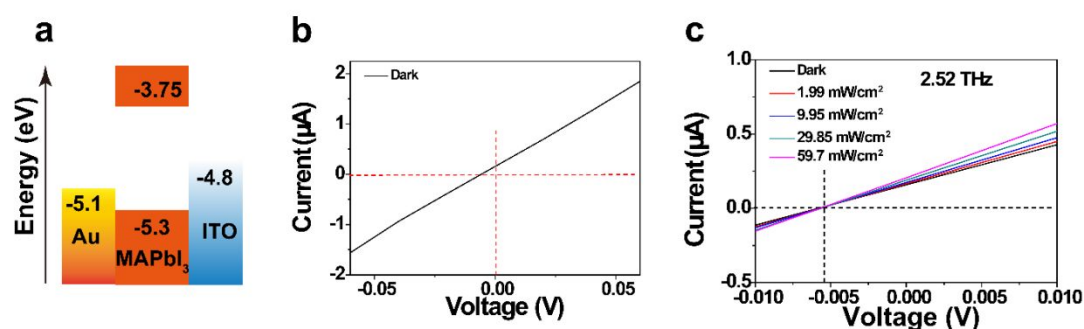


Figure S6 (a) The energy-level diagram of the Au/MAPbI₃/ITO device. (b) I - V curve of the Au/MAPbI₃/ITO device under dark condition. (c) I - V characteristics of the device under different 2.52 THz illumination at -0.01 V to 0.01 V.

Under illumination of 2.52 THz, the device shows almost linear I - V characteristics. Due to the different work functions, the Au electrode forms an Ohmic contact, while,

the interface between perovskite and ITO may form a very small Schottky barrier. **Figure S6a** shows the energy-level diagram of the Au/MAPbI₃/ITO device. Because of the different work functions, an internal electric field can be formed spontaneously in the photodetector channel. **Figure S6b** shows the I-V curve of the device in the dark under the voltage sweep sequence of -1 V → 0 V → 1 V. The open-circuit voltage occurs at about -0.006 V, indicating that the internal electric field is about -0.006 V. The reported result³ of -0.7 V is about 100 times higher than the value of -0.006 V in our Au/MAPbI₃/ITO device. We can speculate that in our Au/MAPbI₃/ITO device a very small Schottky barrier may be formed in the MAPbI₃/ITO junction. Because of fast scanning voltage speed about 2V/s is used in our measuring equipment, the small Schottky barrier is ignored. **Figure S6c** shows the *I-V* characteristics of the device under different 2.52 THz illumination at -0.01 V to 0.01 V.

Therefore, as shown in Figure 2, S2, 3 and Figure 4 of the Au/MAPbI₃/ITO device in our work, the *I-V* characteristics show almost linear relationship between the two electrodes and the MAPbI₃. This may be due to the different halide iodine results in a very small Schottky barrier in the MAPbI₃/ITO junction and the fast scanning voltage speed about 2V/s skipped this small barrier.

As shown in **Figure S6c**, the increase in photocurrent with increasing light intensity can possibly be attributed to changes in resistance generation under IR-THz irradiation. The number of carriers in MAPbI₃ increases with light induced temperature increasing and result in changes in resistance. Specifically, light with higher power

intensity in the IR-THz wavelengths range can produce larger temperature rises, which lead to increased carriers generation and thus contribute to the larger photocurrents.

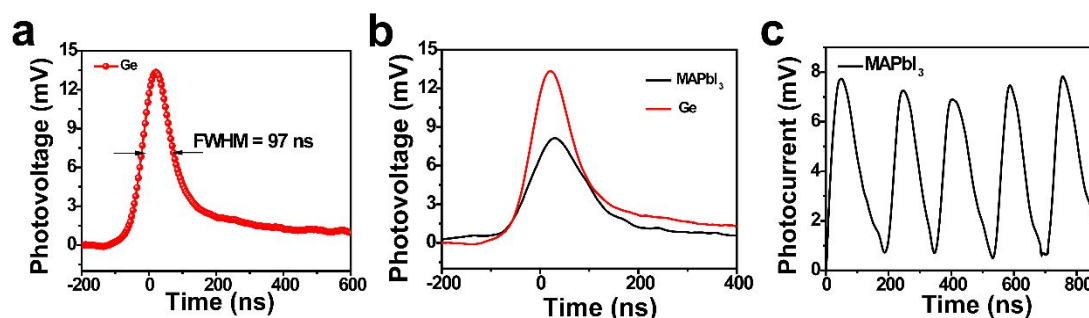


Figure S7. High speed photoresponse characteristic of the MAPbI₃ photodetector. (a) The strong pulsed peak of a single pulse of pulsed laser. (b) Impulse response curves of the device and standard Ge photodetector under 1064 nm pulsed laser. (c) The whole on-off cycles of the device under 1064 nm pulsed laser illumination.

A 1064 nm pulsed laser was used as the source and a beam splitter mirror was used to divide the source light into two beams. In order to ensure the accuracy of detected signals, a commercial Ge detector was used as the standard value optical detector.

Figure S7a shows the single pulse of pulsed laser a strong pulsed peak as triangle with the full width at half maximum (FWHM) of about 97 ns. **Figure S7b** shows the impulse response curves of the MAPbI₃ device and standard Ge PD under 1064 nm pulsed laser illumination. The device's voltage signal corresponds to that of the standard Ge detector, indicating that the device displays a rapid response speed with ns scale time response. Similarly, the MAPbI₃ device exhibits a strong pulsed peak and the uptrend and downtrend correspond to that of the standard Ge detector. The result indicates that the switching curve of MAPbI₃ PD is actual and not distortion. **Figure S7c** displays the complete on-off cycles of the device under 1064 nm pulsed laser illumination. The MAPbI₃ PD exhibits stable and repeatable characteristics under irradiation by multiple

pulses. The above results demonstrate that the MAPbI₃ PD displays a rapid response speed with ns scale time and the response time is scientific and dependable.

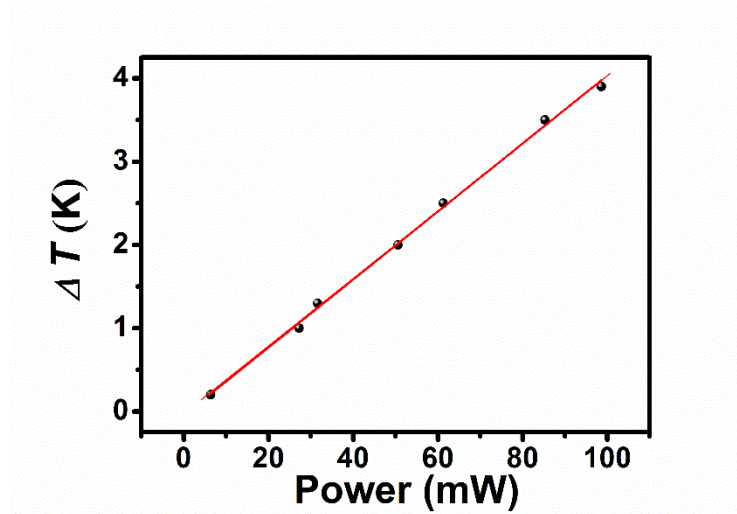


Figure S8 The temperature variation (ΔT) of the MAPbI₃ film as a function of the incident laser power.

The bolometric response time can be calculated by $t \approx R_h C_h$. Where R_h is the thermal resistance and C_h is the heat capacity. **Figure S8** shows the temperature variation (ΔT) of the MAPbI₃ film as a function of the incident 1064 nm laser power P , then thermal resistance can be computed by $R_h = dT/dp \approx 0.04\text{K/mW}$, $C_h \approx 2.5 \times 10^{-9}\text{J/K}$, resulting in the response time $t \approx 100\text{ ns}$. This calculated value confirms the reasonability of the experimental data. The fast response could be attributed to the excellent thermoelectric performance of pure MAPbI₃ and the good contact between the MAPbI₃ and electrodes.

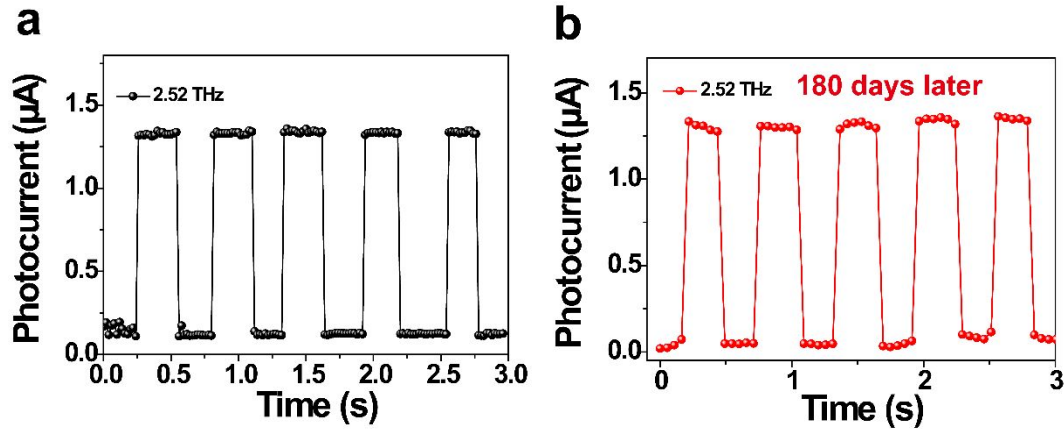


Figure S9 The stability of THz photodetection. Photoresponse curves under 2.52 THz at 1.98 mW/cm² and 0.16 V bias voltage of the (a) original MAPbI₃ photodetector and (b) the MAPbI₃ photodetector 180 days later.

As we all know that perovskites present different phases with the change of temperature. MAPbI₃ presents orthorhombic, tetragonal and cubic phases when the temperature is below 160 K, in the range of 160-330 K and higher than 330 K, respectively.^{4, 5} According to **Figure 5**, the perovskite temperature keeps 21-31 °C under different laser illumination. Therefore, the MAPbI₃ film remains tetragonal phase during testing process.

The stability of THz photodetection was further evaluated by using the MAPbI₃ which was placed in the vacuum chamber for 180 days. **Figure S9a** shows the photocurrent cycles of the original sample and **Figure S9b** is that of 180 days later under the same 2.52 THz radiation ($E_e=1.98$ mW/cm², $V=0.16$ V bias voltage). The device still showed excellent light-switching behavior after 180 days. The photocurrent of the device slightly reduced from 1.31 to 1.29 μA. This result demonstrate THz photodetection stability of the MAPbI₃ photodetector.

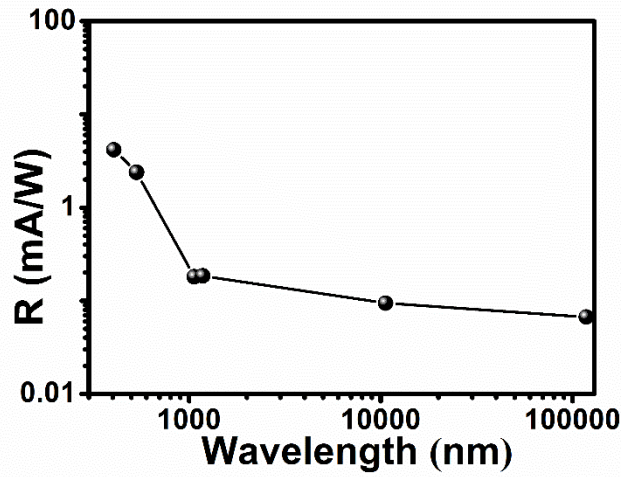


Figure S10 The broadband photoresponsivity over wavelength range from 400 nm to 118 μm at 0.01 V voltage.

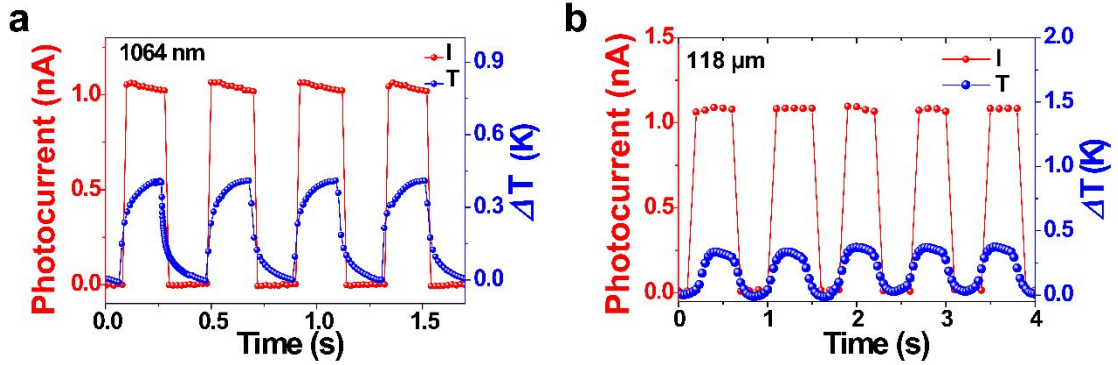


Figure S11 The photocurrent (red line) and temperature (blue line) curves as a function of time at 0 V bias voltage under (a) 1064 nm (108.9 mW/cm^2) and (b) 2.52 THz (1981.7 mW/cm^2) illumination.

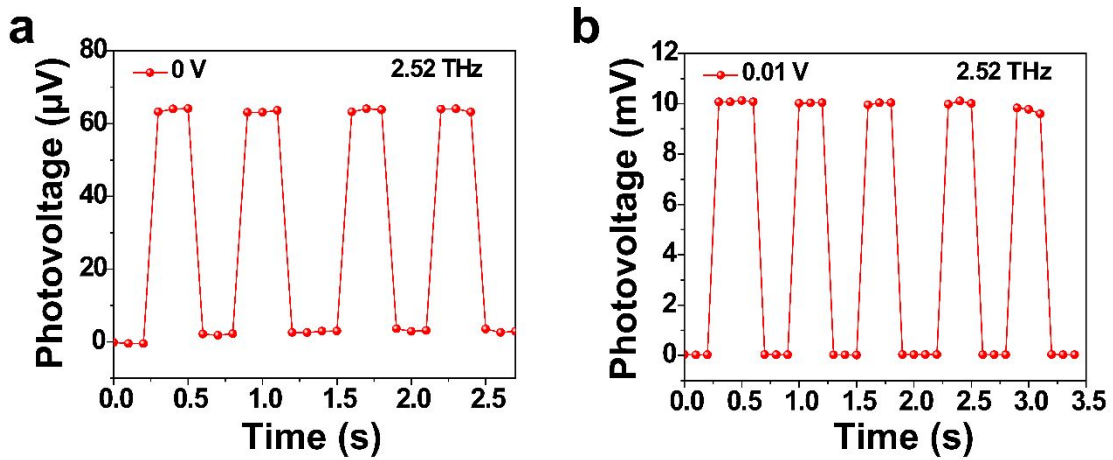


Figure S12 The photovoltage curves of the device at (a) 0 V bias voltage, and (b) 0.01 V bias voltage under 2.52 THz illumination.

For further investigate the THz detection mechanism, we carried out the photovoltage switched curves of the device under 2.52 THz (1981.7 mW/cm²) illumination, as shown in **Figure S12**. The device exhibits photovoltage values of 63.4 μ V at 0 V bias voltage and 10 mV at 0.01 V bias voltage, respectively. As we all know that PTE effect is related to Seebeck coefficient S (in V K⁻¹) and temperature difference, so the PTE voltage is calculated by $V_{\text{PTE}} = \Delta S \Delta T$. In this work, when the device was illuminated by 2.52 THz (1981.7 mW/cm²), the temperature increased by 0.4 K, as shown in **Figure S11** and **Figure 5**. According to **Figure S3**, the Seebeck coefficient of the MAPbI₃ film is about 25 μ V K⁻¹, so the V_{PTE} is about 10 μ V. It is obvious that the PTE voltage accounts for only 15% and 0.1% of the total photovoltage value when the external bias is 0 V and 0.01 V, respectively. For THz response of the MAPbI₃ device, the contribution of PTE effect decreases rapidly with the increase of external bias. Therefore, both of the PTE effect and bolometric effect occurred in the MAPbI₃ device. But, bolometric effect plays a dominant role for the photoresponse and the PTE effect can be almost ignored with the increase of the external bias applied.

METHODS

Synthesis of the MAPbI₃: The MAPbI₃ thin film was grown by using anti-solvent method. The MAPbI₃ perovskite precursor solution was prepared by dissolving a mixture of PbI₂ (99.99%) and MAI (99%) by using a molar ratio of 1:1. The mixture dissolved in a mixed solvent DMF (99.5%) and DMSO (99.5%) with volume ratio of 7:3. The precursor solution was spin-coated on ITO substrate with a rotate speed of 6000 rpm. After a delay time of 15-30 s, the films were dripped in the antisolvent CB

150 μL . Then, the films were firstly in the glove box annealed at 100 $^{\circ}\text{C}$ for 15–30 s. Finally, the perovskite films were fully annealed at 100 $^{\circ}\text{C}$ for 15 min in the air.^{2, 5, 6}

Fabrication process of the Au/ MAPbI₃ /ITO: The Au/ MAPbI₃ /ITO photodetectors were fabricated as follows. A glass sheets coated with indium tin oxid (ITO) film served as the substrate. The ITO/SiO₂ substrate with dimensions of 14×14×2 mm was handled within a UV-ozone system for 15 min. Then the MAPbI₃ perovskite film was spin-coated on ITO/ SiO₂ substrate. After the process was complete, the samples were placed in a vacuum chamber with a vacuum of 10⁻⁴ Pa. The electrodes were then prepared by the thermally evaporation method using shadow mask on the MAPbI₃ perovskite film was made from Cr/Au (10/200 nm).

Characterization and testing: The MAPbI₃'s cross and surface morphologys were examined using scanning electron microscope (SEM) and Atomic Force Microscope (AFM). The structure of the MAPbI₃ film was obtained using X-Ray Powder Diffraction (XRD). The photoluminescence (PL) spectrum was carried out by 374 nm laser. The *I-V* characteristics and the photocurrents of the MAPbI₃ were obtained by using a Keithley 2400 source meter with Labview software. The light sources were 405, 532, 808, 1064, and 1170 nm semiconductor lasers, 9.6, 10, 10.6 μm carbon dioxide (CO₂) gas laser and 118 μm terahertz source (FIRL 100). The light power was measured by using a power meter with an RS232 port (Ophir Vega). The broadband response and the absorption spectra of the device were tested using a Zolix Omni- λ 3007 spectrophotometer with Si and InGaSn photodetectors. The absorption performance of the MAPbI₃ was tested using a terahertz time-domain spectroscopy system. The

temperature distribution image was recorded by the Infrared thermal imager (FLIR T630sc).

Frequency response test of the MAPbI₃ PD: We lowered the laser frequency to obtain the ladder curves by using an optical chopper controller (SR540, STANFORD RESEARCH SYSTEMS, INC, 4 Hz-3.9 KHz) and a continuous wave (CW) 1064 nm laser was used as the laser source. A commercial Ultrafast Ge (UPD-100-IR1-P, ALPHALAS) detector was used to standardize the output laser. **Table S1** shows the parameters of commercial Ultrafast Ge detector. As shown in **Table S1**, the Ultrafast Ge detector exhibits stable and fast (<100 ps) response time. Therefore, in the next process of experiment, the signal measured by the Ultrafast Ge detector is a real laser output signal. Firstly, we used Ge detector to measure the chopper controlled laser signal. **Figure S12a** shows the schematic diagram of the Ge detector test system. **Figure S12b** shows the V-t curves of chopped laser signal from 10 Hz to 3.9 KHz, which was limited by the chopper controller.

Table S1. Parameters of commercial Ultrafast Ge (UPD-100-IR1-P) detector.

Type	Brand	Risetime	Pulsewidth	Wavelength	Others
UPD-100-IR1-P	Alphas	< 100 ps	< 300 ps (FWHM)	400nm- 2000nm	50 Ω load

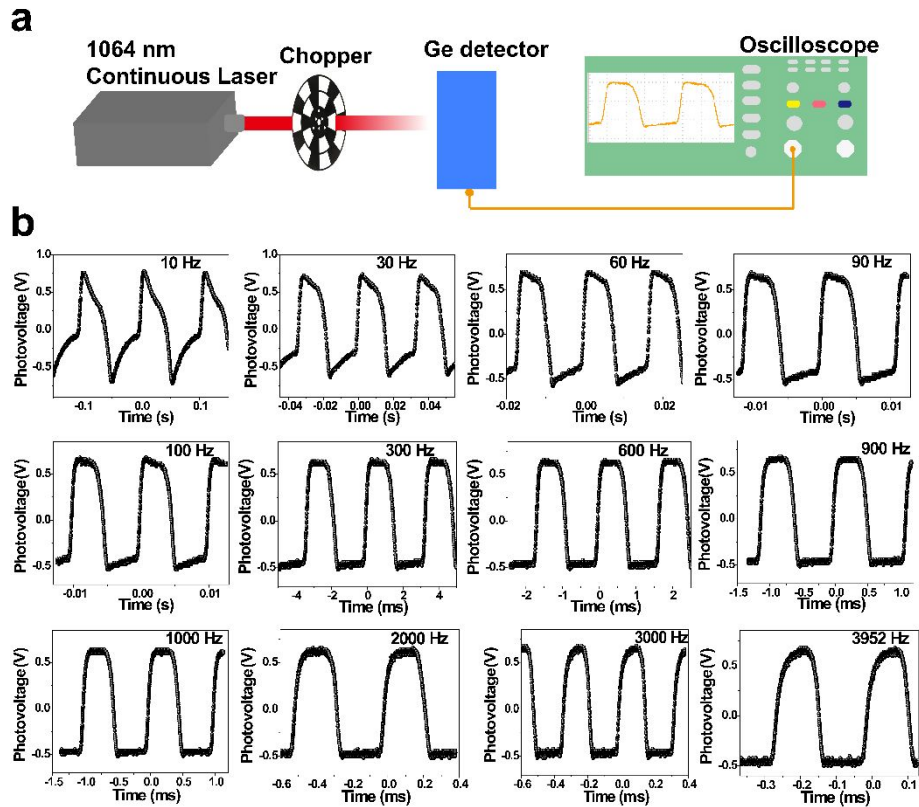


Figure S13 (a) The schematic diagram of Ge detector test system. (b) The chopped laser signal from 10 Hz to 3.9 KHz.

Then, we measured the photoresponses of the MAPbI₃ photodetector. **Figure S13a** shows the schematic diagram of MAPbI₃ detector test system. **Figure S13b** shows the photovoltage-time curves of the MAPbI₃ detector from 10 Hz to 3.9 KHz. It is clearly to see that the shape of curves from 10 Hz to 3.9 KHz in **Figure S13b** are consistent with the chopped laser signals obtained by Ge detector, which indicates no distortion in the waveform of the MAPbI₃ device. Moreover, the responsivity is basically the same in the frequency from 10 Hz to 3.9 KHz. Due to the frequency limitation of chopper controller, the lower frequency test was paused at 3.9 KHz. The above results demonstrate that the response cut-off frequency of MAPbI₃ detector is far more than 3.9 KHz and the response is lower than μ s magnitude.

Crawford, Structures, Phase Transitions and Tricritical Behavior of the Hybrid Perovskite Methyl Ammonium Lead Iodide. *Scientific reports* 2016, 6, 1-16.

5. Saliba, M.; Tan, K. W.; Sai, H.; Moore, D. T.; Scott, T.; Zhang, W.; Estroff, L. A.; Wiesner, U.; Snaith, H. J., Influence of Thermal Processing Protocol upon the Crystallization and Photovoltaic Performance of Organic–Inorganic Lead Trihalide Perovskites. *The Journal of Physical Chemistry C* 2014, 118, 17171-17177.

6. Li, S.; Zhang, F.; Sun, Q.; Li, Z.; Cui, Y.; Ji, T.; Qin, W.; Zhu, F.; Hao, Y., Entire mirror-like perovskite films for high-performance perovskite solar cells: The role of polar anti-solvent sec-pentyl alcohol. *Organic Electronics* 2018, 57, 133-139.